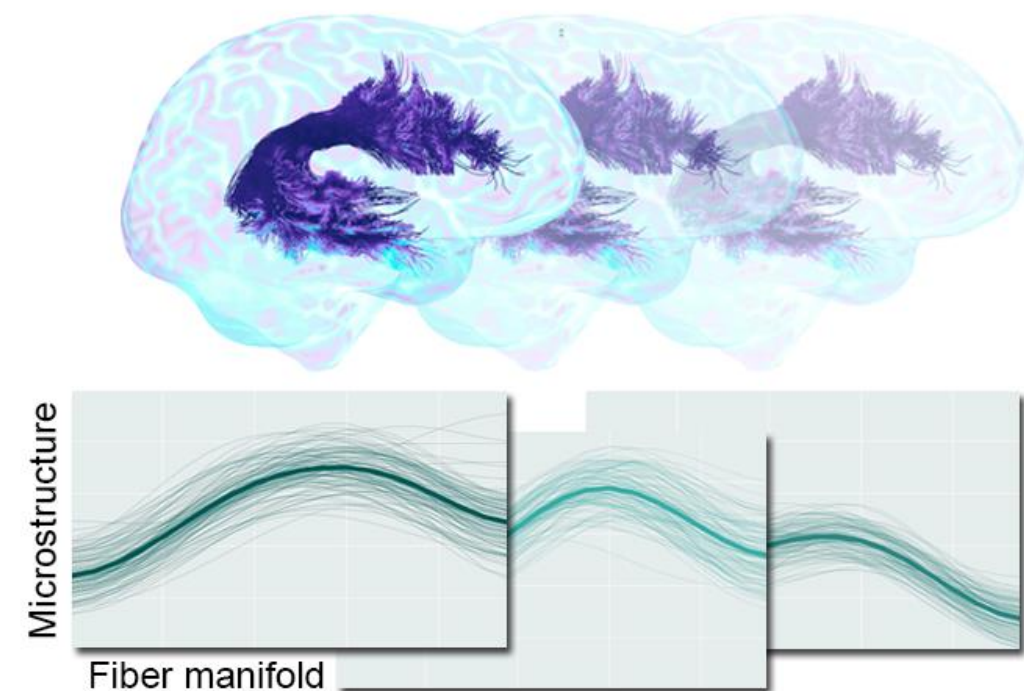


# 1. Introduction

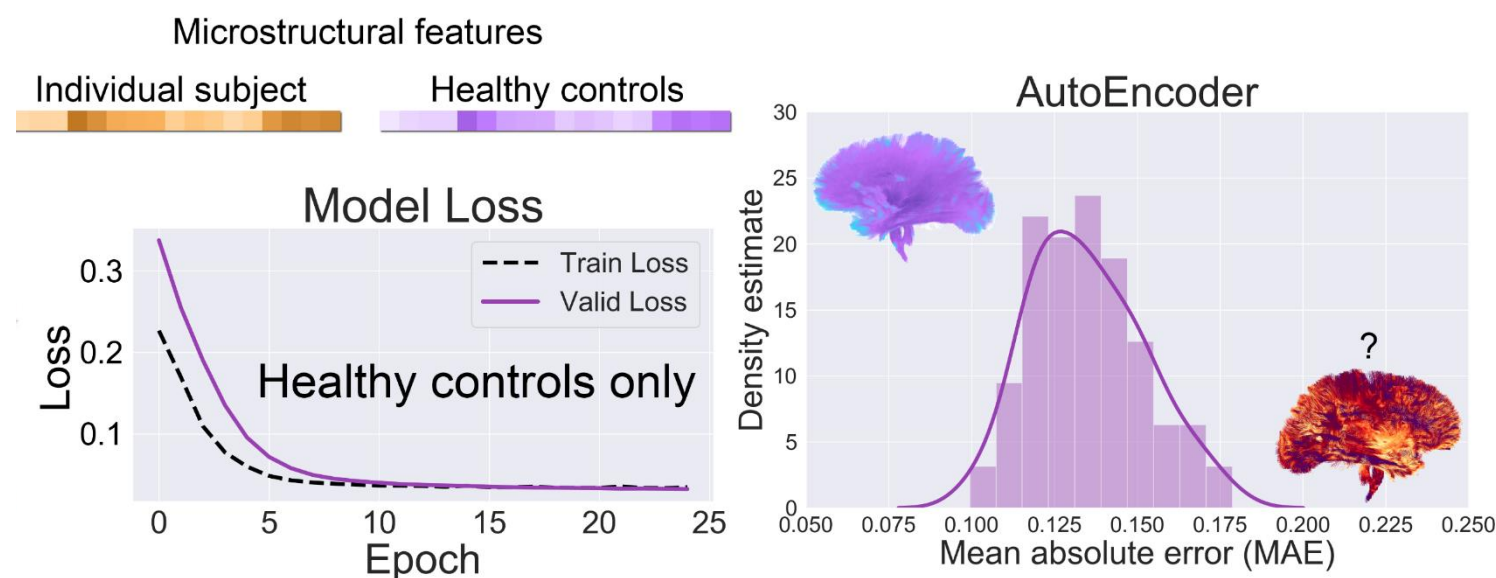
There is an urgent need for a paradigm shift from **group-wise comparisons**<sup>1</sup> (N vs M) to **individual diagnosis** (1 vs M) in diffusion MRI (**dMRI**) to enable the analysis of rare cases and clinically-heterogeneous groups<sup>2</sup>.

**Autoencoders**<sup>3</sup> have the great potential to detect **anomalies** in neuroimaging data<sup>4</sup>.

## Tractometry



## Anomaly detection



[1] Jones, Derek K., and Mara Cercignani. *NMR in Biomedicine* 23.7 (2010): 803-820.  
[2] Marquand, AF., et al. *Biological psychiatry* 80.7 (2016): 552-561  
[3] Hinton, Geoffrey E., and Ruslan R. Salakhutdinov. *science* 313.5786 (2006): 504-507.  
[4] Zimmerer, D et al. MIDL 2019

# 2.1 Methods

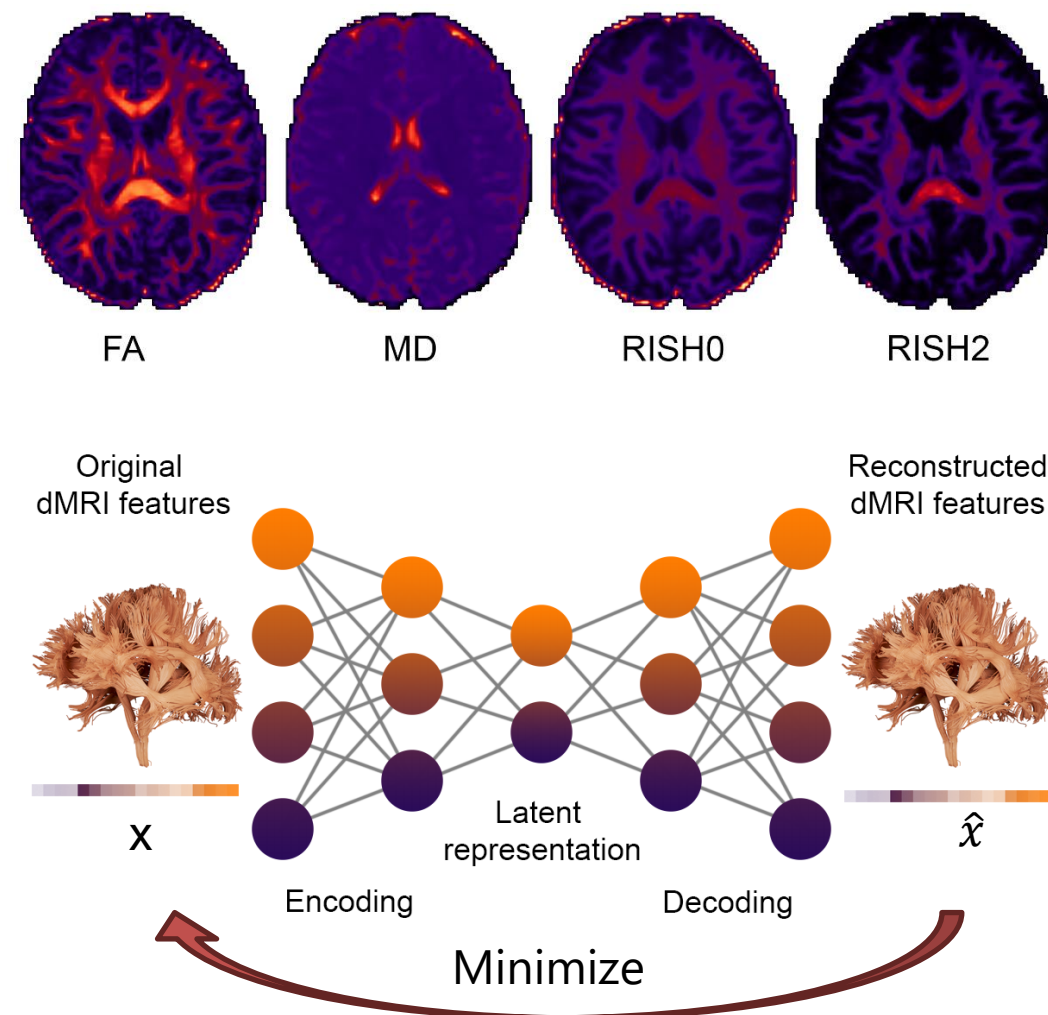
## Dataset

**90** typically developing children (**TD**, 8-18 years)  
**8** children with copy-number variants (**CNV**, 8-15 years)  
 Preprocessed<sup>5</sup> as in *Chamberland et al. 2019*

$2 \times 2 \times 2 \text{ mm}^3$  isotropic voxels and  
 30 diffusion directions at  $b = 500 \text{ s/mm}^2$ ,  
 30 ... at  $b = 1200 \text{ s/mm}^2$ ,  
 60 ... at  $b = 2400 \text{ s/mm}^2$ ,  
 60 ... at  $b = 4000 \text{ s/mm}^2$ ,  
 60 ... at  $b = 6000 \text{ s/mm}^2$  (Siemens 3T **Connectom** scanner @300 mT/m)

## Tractometry

- Automated tract segmentation using TractSeg<sup>6</sup>
- Tractometry<sup>7-9</sup> using **FA**, **MD**, **RISH0** and **RISH2**<sup>10</sup>
- Tract profiles  $\rightarrow$  feature vector
  - $n = 26 \text{ tracts} \times 20 \text{ locations} = 520 \text{ features}$  for each subject.



[5] Chamberland, M, et al. *NeuroImage* 200 (2019): 89-100.

[6] Wasserthal, J, et al. *NeuroImage* 183 (2018): 239-253.

[7] Bells, S. et al. *In Proc ISMRM* 2011.

[8] Cousineau, M. et al. *NeuroImage: Clinical* 16 (2017): 222-233.

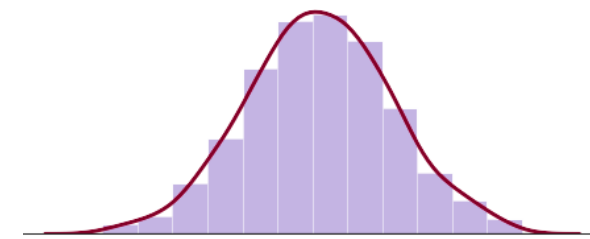
[9] Yeatman, JD., et al. *PloS one* 7.11 (2012).

[10] Mirzaalian, H. et al. *NeuroImage* 135 (2016): 311-323.

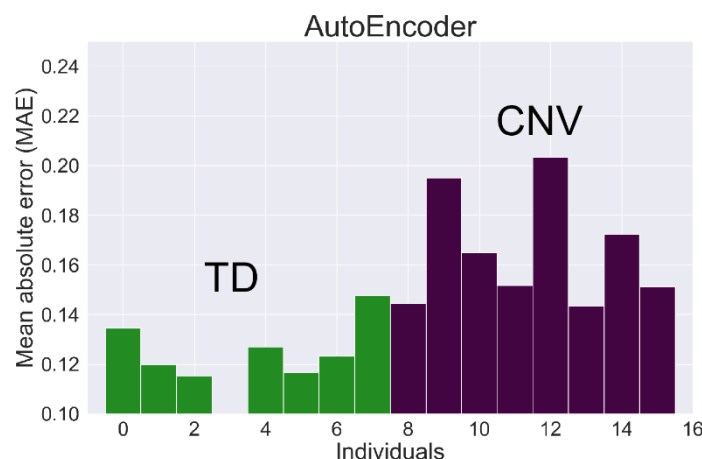
## 2.2 Methods

### Evaluation

- Validation set ( $n = 16$ )  $\rightarrow$  **CNV** ( $n = 8$ ) + a random subset of **TD** ( $n = 8$ ).
- The rest of the **TD** ( $n = 82$ ) data was used to establish a **normative** distribution.
- Anomaly score  $\rightarrow$  mean absolute error (**MAE**) over all features.
- CV shuffle repeat 100 times  $\rightarrow$  derive a mean anomaly score per subject.



$$MAE = \frac{1}{n} \sum_{j=1}^n |y_j - \hat{y}_j|$$



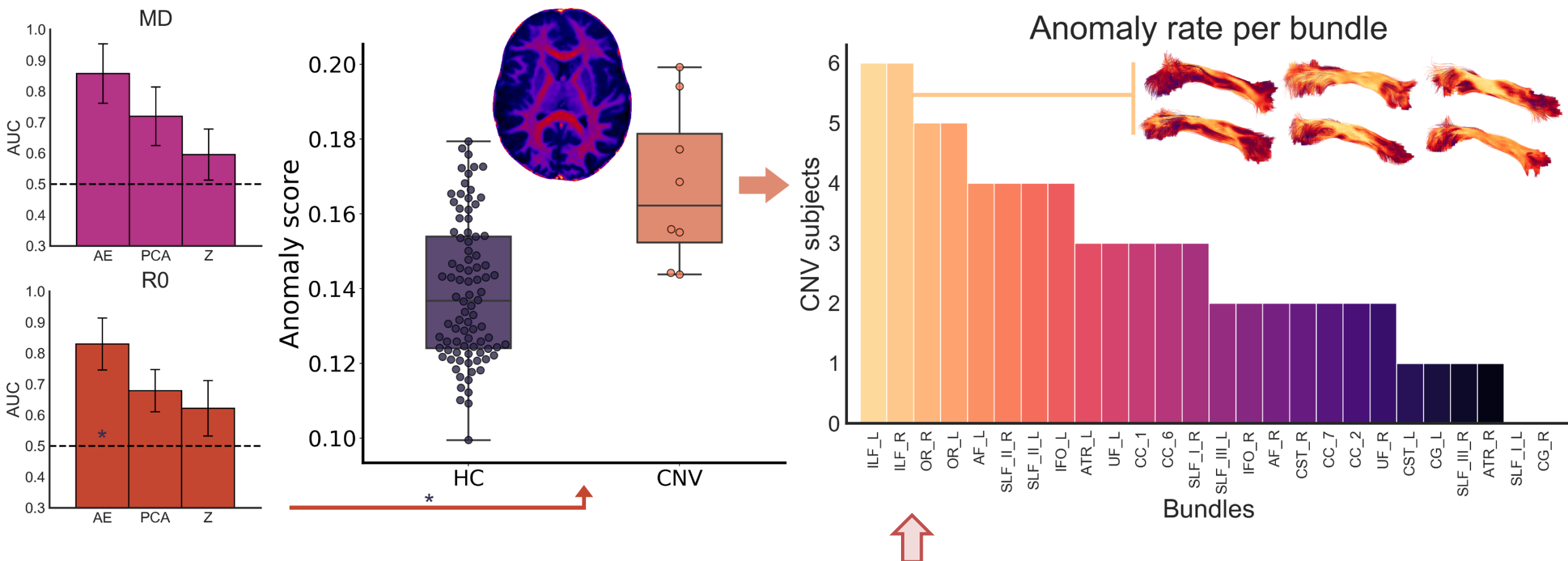
Using the subject labels, we report the mean ROC area under the curve (**AUC**) across the iterations and compared the results with traditional Z-score<sup>9</sup> and PCA<sup>11</sup> approaches.

**Z** vs **M** vs **MAE**  
Univariate Z-score      PCA + Mahalanobis Distance      Autoencoder + Mean Absolute Error

[9] Yeatman, JD., et al. *PLoS one* 7.11 (2012).

[11] Taylor, PN, et al. *Neurology* (2020).

# 3. Results

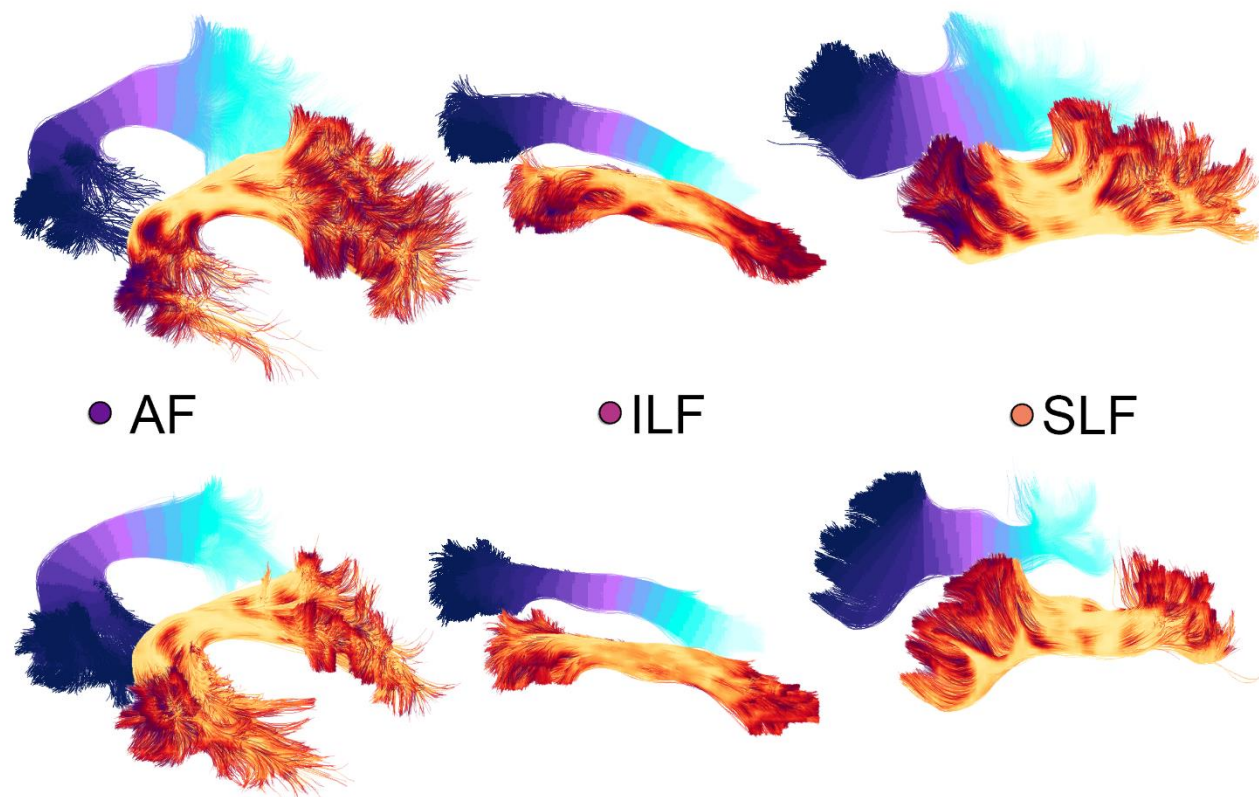
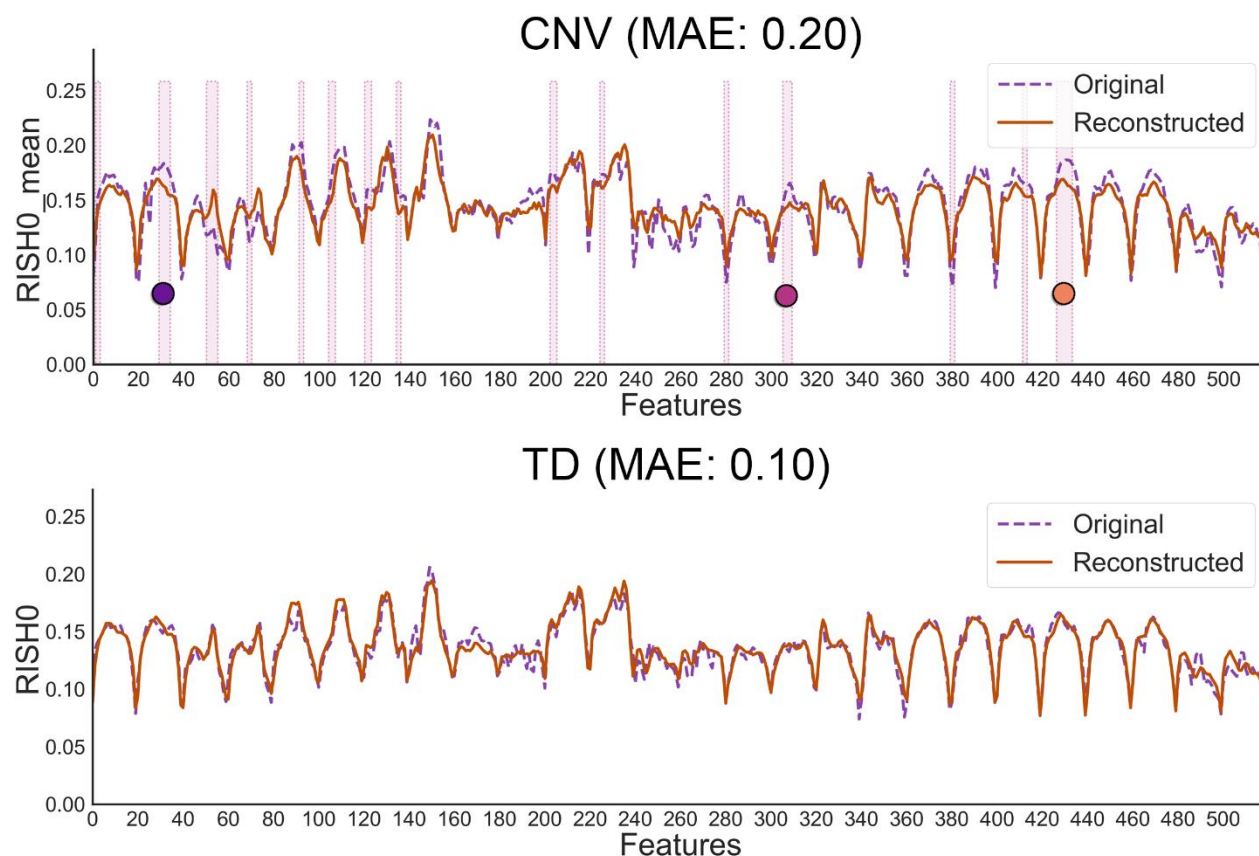


For all four microstructural metrics, the autoencoder approach was better at identifying CNV subjects as outliers, providing substantially higher sensitivity-specificity trade-offs.

Anomalies mostly occurred along the **ILF** and **OR** bundles (bilateral).



# 4. Feature inspection



A key **advantage** of using deep autoencoders for anomaly detection over traditional PCA-derived approach is their unique ability to interpret anomaly scores based on **feature** inspection.

Peer-reviewed short paper (@MIDL2020):  
[arxiv.org/abs/2005.11082](https://arxiv.org/abs/2005.11082)